

# Universal Dynamics of Phase-Field Models for Dendritic Growth

Yung-Tae Kim<sup>1</sup>, Nikolas Provatas<sup>1,2</sup>, Nigel Goldenfeld<sup>1</sup>, and Jonathan Dantzig<sup>2</sup>

<sup>1</sup>University of Illinois at Urbana-Champaign, Department of Physics  
1110 West Green Street, Urbana, IL, 61801

<sup>2</sup>University of Illinois at Urbana-Champaign, Department of Mechanical and Industrial Engineering  
1206 West Green Street, Urbana, IL, 61801

(December 5, 2017)

We compare time-dependent solutions of different phase-field models for dendritic solidification in two dimensions, including a thermodynamically consistent model and several ad hoc models. The results are identical when the phase-field equations are operating in their appropriate sharp interface limit. The long time steady state results are all in agreement with solvability theory. No computational advantage accrues from using a thermodynamically consistent phase-field model.

PACS Numbers: 81.10.Aj, 05.70.Ln, 64.70.Dv, 81.30.Fb

Dendrites are the most commonly observed solidification microstructures in metals. The free growth of a single dendrite is a prototype for problems of pattern selection in materials science [1–5] and has been extensively studied experimentally and theoretically. It is still not possible to compare theory with experiment because of the difficulties in computing three dimensional microstructures in the temperature and material’s parameter range of the experiments.

Recently, a significant step forward was taken by Karma and Rappel [6,7], who not only showed how to compute accurately two dimensional dendritic growth but also were able to compare their results with theoretical predictions. Their calculations used the so-called *phase-field* formulation of solidification, in which a mathematically sharp solid-liquid interface is smeared out or regularized and treated as a boundary layer, with its own equation of motion. The resulting formulation, described in more detail below, no longer requires front tracking and the imposition of boundary conditions, but must be related to the sharp interface model by an asymptotic analysis. In fact, there are many ways to prescribe a smoothing and dynamics of a sharp interface consistent with the original sharp interface model, so that there is no unique phase-field model, but rather a family of related models. An important part of Karma and Rappel’s work was an improved asymptotic analysis which allows coarser spatial grids to be used in the numerical computations than was previously possible.

Although the phase-field method has gained acceptance as a useful way to study solidification problems, a debate still exists over the interpretation and validity of the phase-field models themselves. Each model includes a double-well potential field which enforces the above properties of the phase-field. Some models can be shown rigorously to satisfy entropy inequality [8,9]. These are sometimes called “thermodynamically consistent” models. On the other hand, it has been argued that the precise form of the phase-field equations should be irrelevant so long as the computations are performed

at the asymptotic limit where the phase-field model converges to the sharp interface limit [10].

The purpose of this Letter is to compare the dynamics of the different phase-field models proposed. To this end, we have performed accurate and extensive computations using a specially developed adaptive mesh refinement algorithm [11,12]. We find that when properly used, all phase-field models give precisely equivalent results; not only does each phase-field model converge to the steady state predicted by theory, but also the transient dynamics approach the steady state uniquely. Indeed, once one has established that there is genuine universal dynamic behavior, the only remaining consideration is the computational efficiency. Our results clearly indicate that the CPU times required for the different models are identical. In particular, we find no advantage for the thermodynamically consistent model.

A secondary purpose of this Letter is to detect the limit of the validity of phase-field models in describing the sharp interface problem. In the context of the asymptotic analysis of Karma and Rappel [6,7], the ratio of the interface width to the diffusion length (referred to as the interface Péclet number, IPe) must be small in order for the different phase field-models to collapse to identical free-boundary problems. We show how finite-IPe discrepancies encountered between different models can be eliminated by adjusting the phase-field parameters. We emphasize that IPe is a free parameter and can be varied for numerical convenience by changing the interface width.

The solidification of a pure substance is described by a free-boundary problem for the temperature in the solid and liquid phases, and the position of the interface between them:

$$\partial_t u = D \nabla^2 u \quad (1)$$

$$V_n = D(\partial_n u|^+ - \partial_n u|^-) \quad (2)$$

$$u_i = -d(\vec{n})\kappa - \beta(\vec{n})V_n \quad (3)$$

The temperature  $T$  has been rescaled as a dimensionless thermal field  $u = (T - T_m)/(L/C_p)$ , where  $T_m$ ,  $L$ , and

$C_p$  represent the melting temperature, the latent heat of fusion, and the specific heat at constant pressure, respectively. The thermal diffusivity  $D$  in Eq. (1) is assumed to be equal in both phases. Eq. (2) describes energy conservation at the solid-liquid interface, where  $V_n$  is the local outward normal interface velocity and  $\partial_n$  refers to the outward normal derivative at the interface for the solid (+) and liquid (-) phases. Finally, Eq. (3) is known as the Gibbs-Thomson condition, describing the deviation of the interface temperature  $u_i$  from equilibrium, due to the local curvature  $\kappa$ , and interface kinetics.  $d(\vec{n}) = \gamma(\vec{n})T_m C_p / L^2$  is the anisotropic capillary length, proportional to the surface tension  $\gamma(\vec{n})$ , and  $\beta(\vec{n})$  is the anisotropic kinetic coefficient.

Eqs. (1)-(3) have been studied extensively to determine the steady state features of dendritic growth [3–5]. These equations admit a family of discrete solutions. Only the fastest growing of this set of solutions is stable, and this is the dynamically selected “operating state” for the dendrite, corresponding to a unique tip shape and tip velocity. This theoretical treatment is usually called solvability theory. Recent calculations of dendritic growth using phase-field models have been found to be in good agreement with the predictions of solvability theory [6,7,11].

The phase-field model finesses the computational difficulties associated with front-tracking on a discrete lattice by introducing an auxiliary continuous order parameter, or phase-field,  $\phi(\mathbf{r}, t)$  that couples to the evolution of the thermal field. The dynamics of  $\phi(\mathbf{r}, t)$  are designed to follow the evolving solidification front [13–19]. The phase-field interpolates between the solid and liquid phases, attaining a different constant value in each phase (typically  $\pm 1$ ), with a rapid transition region in the vicinity of the solidification front. The liquid-solid interface is defined by the level set of  $\phi(\mathbf{r}, t) = 0$ .

We consider phase-field equations of the form

$$\begin{aligned} \frac{\partial u}{\partial t} &= D \nabla^2 u + \frac{1}{2} \frac{\partial h(\phi)}{\partial t} & (4) \\ \tau(\vec{n}) \frac{\partial \phi}{\partial t} &= \nabla \cdot (W^2(\vec{n}) \nabla \phi) - \frac{F(\phi, \lambda u)}{\partial \phi} \\ &+ \frac{\partial}{\partial x} \left( |\nabla \phi|^2 W(\vec{n}) \frac{\partial W(\vec{n})}{\partial \phi_x} \right) \\ &+ \frac{\partial}{\partial y} \left( |\nabla \phi|^2 W(\vec{n}) \frac{\partial W(\vec{n})}{\partial \phi_y} \right), & (5) \end{aligned}$$

as in Refs. [6,7]. The order parameter is defined by  $\phi$ , with  $\phi = +1$  in the solid, and  $\phi = -1$  in the liquid. The interface is defined by  $\phi = 0$ .

The function  $F(\phi, \lambda u) = f(\phi) + \lambda u g(\phi)$  is a phenomenological free energy where  $f(\phi)$  has the form of a double-well potential,  $\lambda$  controls the coupling between  $u$  and  $\phi$ , and the relative height of the free energy minima is determined by  $u$  and  $g(\phi)$ . The function  $h(\phi)$  accounts for the liberation of latent heat. Anisotropy has been introduced in Eq.(5) by defining  $W(\vec{n}) = W_o A(\vec{n})$  and  $\tau(\vec{n}) = \tau_o A^2(\vec{n})$ .  $\tau_o$  is a time characterizing atomic

movement in the solid-liquid interface,  $W_o$  is a length characterizing the width of the interface, and

$$A(\vec{n}) = (1 - 3\epsilon) \left[ 1 + \frac{4\epsilon}{1 - 3\epsilon} \frac{(\phi_{,x})^4 + (\phi_{,y})^4}{|\nabla \phi|^4} \right] \quad (6)$$

with  $A(\vec{n}) \in [0, 1]$ .  $\phi_{,x}$  and  $\phi_{,y}$  represent partial derivatives with respect to  $x$  and  $y$ , and the vector  $\vec{n} = (\phi_{,x} \hat{x} + \phi_{,y} \hat{y}) / (\phi_{,x}^2 + \phi_{,y}^2)^{1/2}$  is the normal to the contours of  $\phi$ . The constant  $\epsilon$  parameterizes the deviation of  $W(\vec{n})$  from  $W_o$  and is a measure of the anisotropy strength.

We use the asymptotic relationships of Karma and Rappel [6,7] to map the phase-field model into the free-boundary problem, where Eqs. (4) and (5) reduce to Eqs. (1)-(3). In terms of  $A(\vec{n})$ ,  $\beta(\vec{n}) = \beta_o A(\vec{n})$  and  $d(\vec{n}) = d_o [A(\vec{n}) + \partial_\theta^2 A(\vec{n})]$ , where  $\theta$  is the angle between  $\vec{n}$  and the  $x$ -axis; noting that  $\tan(\theta) = \phi_{,y} / \phi_{,x}$ , these expressions become  $\beta(\vec{n}) = \beta_o (1 + \epsilon \cos 4\theta)$  and  $d(\vec{n}) = d_o (1 - 15\epsilon \cos 4\theta)$  in the free-boundary problem. The parameters of the phase-field model are related to the free-boundary parameters by  $\lambda = W_o a_1 / d_o$  and  $\tau_o = W_o^3 a_1 a_2 / (d_o D) + W_o^2 \beta_o / d_o$ . The positive constants  $a_1$  and  $a_2$  depend on the exact form of the phase-field equations. In choosing to simulate particular material characteristics, we fix the experimentally measurable quantities  $d_o$ ,  $\beta_o$ , and  $D$ , leaving  $W_o$  as a free parameter which determines  $\lambda$  and  $\tau_o$ .

We compute four-fold symmetric dendrites in a quarter-infinite space using a new finite-element adaptive grid method reported in Refs. [11,12]. Solidification is initiated by a small quarter disk of radius  $R_o$  centered at the origin. The order parameter is initially set to its equilibrium value  $\phi_o(\vec{x}) = -\tanh(|\vec{x}| - R_o) / \sqrt{2}$  along the interface. The initial temperature is  $u = 0$  in the solid and decays exponentially from  $u = 0$  at the interface to  $u = -\Delta$  as  $\vec{x} \rightarrow \infty$ , where the far-field *undercooling* is  $\Delta = (T_m - T_\infty) / (L / C_p)$  and  $T_\infty$  is the temperature far ahead of the solidification front in the liquid.

The different phase-field models we study are summarized in Table I. To satisfy the asymptotics,  $f(\phi)$  is chosen to be an even function, and  $g(\phi)$  and  $h(\phi)$  are odd. For all of the models,  $f(\phi) = \phi^4 / 4 - \phi^2 / 2$ . For computational purposes, the  $g(\phi)$  are chosen such that the two minima of  $F(\phi, \lambda u)$  are fixed at  $\phi = \pm 1$ . Model 1 is a form used by Almgren [20], Model 2 is a form used by Karma and Rappel [6,7], and Model 5 is the thermodynamically consistent form used by Wang et al [9]. Models 3 and 4 are forms created by us that meet the

TABLE I. Summary of phase-field models studied.

Model	$\frac{\partial g(\phi)}{\partial \phi}$	$h(\phi)$	$a_1$	$a_2$
1	$1 - \phi^2$	$\phi$	$\frac{1}{\sqrt{2}}$	$\frac{5}{6}$
2	$(1 - \phi^2)^2$	$\phi$	$\frac{5}{4\sqrt{2}}$	$\frac{47}{75}$
3	$(1 - \phi^2)^3$	$\phi$	1.0312	0.52082
4	$(1 - \phi^2)^4$	$\phi$	1.1601	0.45448
5	$(1 - \phi^2)^2$	$\frac{15}{8}(\phi - \frac{2}{3}\phi^3 + \frac{1}{5}\phi^5)$	$\frac{5}{4\sqrt{2}}$	0.39809

TABLE II. Summary of simulation parameters.

$\Delta$	$L$	$R_o$	$\Delta x$	$\Delta t$	$D$	$d_o$	$\tilde{V}$	IPe
0.45	1000	17	0.39	0.010	3	0.5	0.00545	0.011
0.55	800	15	0.39	0.016	2	0.5	0.0170	0.034
0.65	800	15	0.39	0.016	1	0.5	0.0469	0.094
0.65	800	15	0.39	0.004	2	1.5	0.0469	0.031

above requirements. It should be noted that Model 1 requires that  $\lambda < 1/\Delta$  otherwise the  $\phi = -1$  state becomes linearly unstable.

In our simulations, the computational domain is an  $L \times L$  square box. Computations were performed at  $\Delta = 0.65, 0.55$ , and  $0.45$ . A summary of the parameters used for each simulation is given in Table II, where  $\tilde{V} = Vd_o/D$  is the dimensionless tip velocity predicted by solvability theory,  $\Delta x$  is the *minimum grid spacing* of our mesh [11,12], and  $\Delta t$  is the simulation time step. The phase-field parameters were chosen for each model so that they all simulated the same free-boundary problem. For all simulations  $\epsilon = 0.05$ ,  $\beta_o = 0$ , and  $W_o = 1$ . Figure 1 shows the dimensionless tip velocity of the dendrite versus time for the simulations performed at  $\Delta = 0.55$  and  $0.45$ . These results show that all of the phase-field models studied produce identical results for the entire temporal evolution of the dendrite and also converge to steady state solutions that are within a few percent of those predicted by solvability theory. In addition, the CPU times required for each of the models were identical.

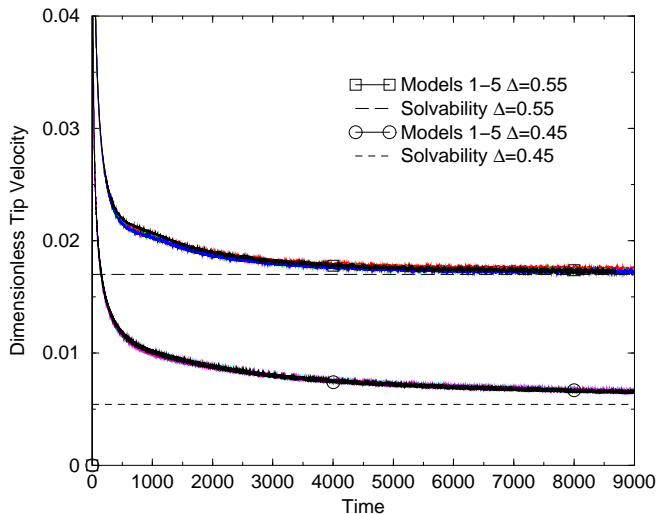


FIG. 1. Time evolution of the dimensionless tip velocity for five different phase-field models at  $\Delta = 0.55$  and  $0.45$ . Each curve consists of five solutions superimposed on one another.

At  $\Delta = 0.65$  (with  $d_o = 0.5$ ), however, there are significant quantitative differences between the various phase-field models, as shown in Fig. 2. This discrepancy is attributed to finite-IPe corrections at higher order in the asymptotic expansion. The deviations are a signal that

the solutions have not converged as a function of the expansion parameter and that the phase-field equations are not operating within the sharp interface limit. It should be possible to make these higher order terms negligible if one makes IPe smaller. Figure 2 also shows that each model has different convergence properties. However, in other simulations we have found that no single model consistently converges more rapidly than the others; in general, the convergence appears to depend on the initial conditions.

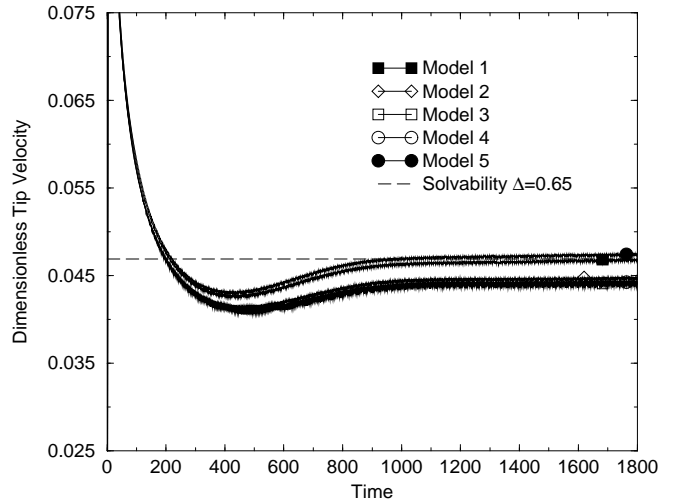


FIG. 2. Time evolution of the dimensionless tip velocity for five phase-field models at  $\Delta = 0.65$  with  $d_o = 0.5$  and  $IPe = 0.094$ . When IPe is too large the different models do not exhibit universal behavior.

In their asymptotic analysis, Karma and Rappel expand the solutions to the phase-field equations treating the interface Péclet number as a small parameter [6,7]. This expansion parameter can be written as  $IPe = WV/D = W_o\tilde{V}/d_o$ , where the dimensionless velocity  $\tilde{V}$  depends *only* on  $\Delta$  and  $\epsilon$ . We decreased IPe for the  $\Delta = 0.65$  case by simulating with a larger value of  $d_o$ . Figure 3 shows the tip velocity versus time for the different phase-field models at  $\Delta = 0.65$  with the capillary length  $d_o = 1.5$ . The universal behavior of the different models is recovered after this adjustment is made.

We have demonstrated that one can obtain identical results from different phase-field models by choosing the expansion parameter IPe to be sufficiently small. Unfortunately, in practice, the interface width is the only parameter that can be used to control the size of IPe, since  $\tilde{V}$  is fixed for a given  $\Delta$  and  $\epsilon$ , and  $d_o$  is set by the particular material to be simulated. Thus, there is only the one free parameter,  $W_o$ , that can be adjusted to make IPe smaller. This restriction can hinder computational efficiency, as the number of grid points necessary to resolve the interface (and thus the simulation time) scales as  $1/W_o^2$  on an adaptive grid, and as  $1/W_o^3$  on a fixed grid. In addition, with zero interface kinetics,  $\tau_o \sim W_o^3$  which places a restriction on the computational

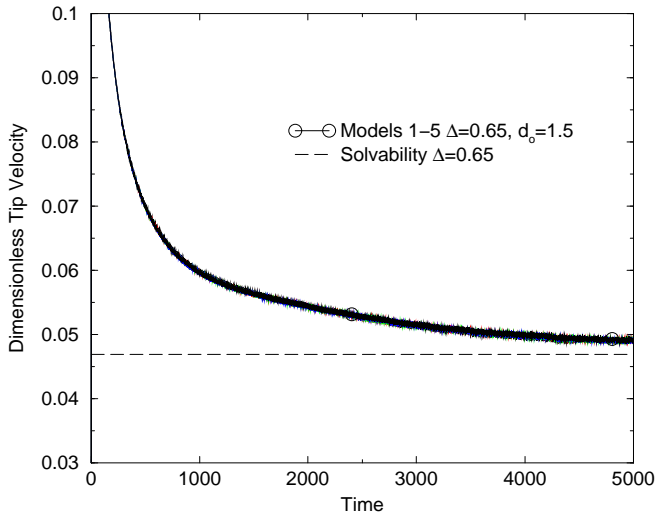


FIG. 3. Time evolution of the dimensionless tip velocity for five phase-field models at  $\Delta = 0.65$  with  $d_o = 1.5$  and  $\text{Ipe} = 0.031$ . Decreasing  $\text{Ipe}$  recovers universal behavior.

time step if an explicit scheme is used. For the simulation at  $\Delta = 0.65$  with  $d_o = 0.5$ , an  $\text{Ipe} = 0.031$  can be obtained by reducing  $W_o$  by a factor of 3, but this would require an impractical amount of computing time. We note that the asymptotics of Karma and Rappel become most accurate at lower undercoolings [12], which is also an experimentally relevant regime. At low  $\Delta$ ,  $\tilde{V} \sim \Delta^4$ , allowing the use of larger values for  $W_o/d_o$ . Simulating at low  $\Delta$  requires larger system sizes. This, however, adds very little computational complexity for adaptive mesh based codes.

We can extend the range of validity for these phase-field models by carrying out the asymptotic analysis further so that finite- $\text{Ipe}$  corrections are pushed to higher orders. This will lessen the restrictions on the interface width, thus rendering the phase-field approach computationally more efficient. Detailed results will be presented in a forthcoming paper [21]. There appears to be a general trend that as one goes to higher orders in the asymptotic expansion more constraints are required on the functions  $f(\phi)$ ,  $g(\phi)$ , and  $h(\phi)$  in order to get rid of correction terms inconsistent with the free-boundary formulation. These constraints can cause the phase-field to have solutions that are not monotonic in the interfacial region, thus requiring higher grid resolution and computation time [20]. We are currently pursuing the development of a phase-field model from a renormalization group approach with the goal of creating a more systematic convergence to the free-boundary problem.

We thank Wouter-Jan Rappel for providing the solvability code used to test some of our simulations, and Alain Karma for generously providing us with his unpublished results. This work has been supported by the NASA Microgravity Research Program, under Grant NAG8-1249. We also acknowledge the support of the National Center for Supercomputing Applications (NCSA)

for the use of its computer resources.

- 
- [1] S.-C. Huang and M. Glicksman. *Acta Metall.* **29**, 1697 (1981).
  - [2] M. E. Glicksman. *Materials Science and Engineering* **65**, 45 (1984).
  - [3] J. Langer. *Rev. Mod. Phys.* **52**, 1 (1980).
  - [4] J. Langer. In *Chance and Matter, Les Houches Session XLVI*, edited by J. V. J. Souletie and R. Stora, 629 (North Holland, Amsterdam, 1987).
  - [5] D. A. Kessler, J. Koplik and H. Levine. *Adv. Phys.* **37**, 255 (1988).
  - [6] A. Karma and W.-J. Rappel. *Phys. Rev. E* **53**, 3017 (1995).
  - [7] A. Karma and W.-J. Rappel. *Phys. Rev. E* **57**, 4323 (1998).
  - [8] O. Penrose and P. C. Fife. *Physica D* **43**, 44 (1990).
  - [9] S.-L. Wang, R. F. Sekerka, A. A. Wheeler, B. T. Murray, S. R. Coriell, R. J. Braun and G. B. McFadden. *Phys. Rev. E* **69**, 189 (1993).
  - [10] J. S. Langer. In *Directions in Condensed Matter*, 164 (World Scientific, Singapore, 1986).
  - [11] N. Provatas, N. Goldenfeld and J. Dantzig. *Phys. Rev. Lett.* **80**, 3308 (1998).
  - [12] N. Provatas, N. Goldenfeld and J. Dantzig. *J. Comp. Phys.* (1998). In press.
  - [13] G. Caginalp. *Arch. Rat. Mech. Anal.* **92**, 205 (1986).
  - [14] J. B. Collins and H. Levine. *Phys. Rev. B* **31**, 6119 (1985).
  - [15] J. A. Warren and W. J. Boettinger. *Acta Metall. Mater. A* **43**, 689 (1995).
  - [16] A. Karma. *Phys. Rev. E* **49**, 2245 (1994).
  - [17] A. A. Wheeler, G. B. McFadden and W. J. Boettinger. *Proc. Royal Soc. London A* **452**, 495 (1996).
  - [18] R. Kobayashi. *Physica D* **63**, 410 (1993).
  - [19] S.-L. Wang and R. F. Sekerka. *Phys. Rev. E* **53**, 3760 (1996).
  - [20] R. Almgren. Preprint (1998).
  - [21] Q. Hou, N. Provatas, Y.-T. Kim, N. Goldenfeld and J. Dantzig. Manuscript in preparation.